ETH
Eidgenössische Technische Hochschule Zürich
Swiss Federal Institute of Technology Zurich

D PHYS

Ulrich Sauter
17-935-966

Gain characterization of pump DBR VECSEL in the 2-µm range

Semester project

Ultrafast Laser Physics, Prof. Ursula Keller
Department of Physics, Institute for Quantum Electronics
Swiss Federal Institute of Technology Zürich

Supervision

Marco Gaulke

May, 2023

Abstract

A novel optically-pumped vertical external cavity surface emitting laser (VECSEL) operating in the 2 µm spectral range

In order to gain deeper insights into the impact of VECSEL design (?MENTION WHAT CHANGES IN DESIGN?), it is necessary to measure the characteristic parameters of the VECSEL under various conditions. This involved utilizing an existing setup and control software to measure these parameters at various temperatures and pump powers. To enhance efficiency and save valuable measurement time, the setup was further improved by adding the possibility to control and automate the pump diode power, aswell as further improvement to the stability and detection algorithm of the software.

Contents

Chapter 1

Introduction

Semiconductor lasers present a very compact compact, efficient and mass producible solid state laser. They have many applications in everyday life and science, such as optical communication, data storage, printing, sensing, medical treatment, and pumping solid-state lasers.

A special type of semiconductor laser is a VECSEL (Vertical External Cavity Surface Emitting Laser). It is based on a VCSEL (Vertical Cavity Surface Emitting Laser) and emits light perpendicular to the surface of a semiconductor wafer but unlike a VCSEL, a VECSEL has an external cavity that is formed by one or more optical elements outside the wafer. This allows for more flexibility in designing the laser parameters, such as wavelength, output power, beam quality and pulse duration.

The basic structure of the VECSEL itself consists of an active region and a distributed Bragg reflector (DBR). Inside the active region, multiple quantum wells are located which are engineered to provide the necessary energy levels for the desired wavelength of laser emission, in this case the 2-µm range. This wavelength range is of strong interest for many application, particularly for medical purposes and atmospheric spectroscopy. The DBR is made of alternating layers of semiconductor material with different refractive indices. By choosing the layer thicknesses to be one quarter of the laser wavelength, the DBR achieves high reflectivity at the desired wavelength range of the laser.

A novel design approach incorporates a DBR for the pump wavelength as well. This new structure shows remarkable improvements in terms of efficiency and power scaling in continuous wave (CW) operation, as seen in Fig. 1.1. The performance improvements in a modelocked configuration were not as significant. To get a better understanding of this, additional investigation were conducted and for this work we focused on the gain saturation characteristics.

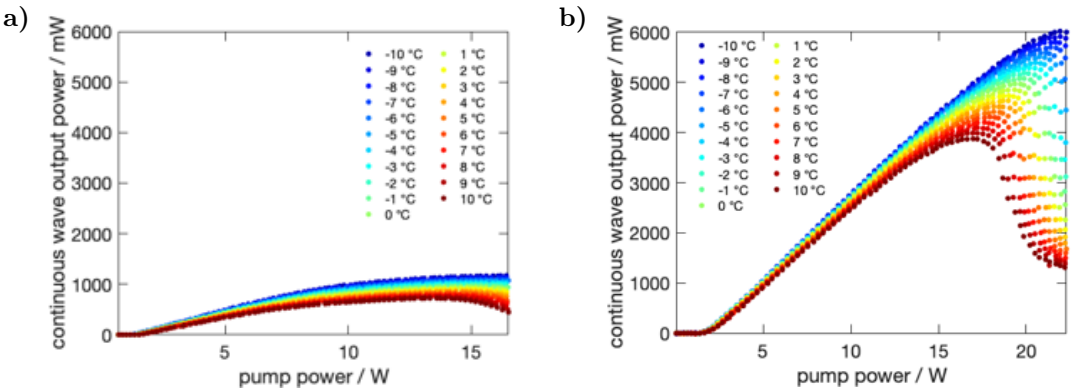

Figure 1.1: Continuous wave (CW) output power of a VECSEL without pump DBR a) and with pump DBR b) versus pump power under different heat sink temperature ranging from $-10\,°C$ to $10\,°C$. The data demonstrates the effect of the pump DBR on the power scaling performance in CW operation. The VECSEL with pump DBR shows an increase of 18 % and a sixfold increase in output power.

1.1 Gain saturation

Gain saturation describes a phenomenon that occurs when the active region of a laser is unable to maintain its gain as the pump power increases for high values.

To study this behaviour, one measures the nonlinear behaviour of the reflectivity for an increasing amount of probe fluence, as can be seen in Fig. 1.2. To quantify this behaviour and gain some macroscopic parameters, a model based on the saturation of the absorber in a SESAM can be fitted to the data.

$$R(F) = R_{ns}\frac{F_{sat}}{F}\ln\left\{1+\frac{R_{ss}}{R_{ns}}\left[\exp\left(\frac{F}{F_{sat}}\right)-1\right]\right\}\exp\left(-\frac{F}{F_2}\right) \tag{1.1}$$

The parameters from Eq. (1.1) are the saturation fluence F_{sat}, the small signal reflectivity R_{ss}, the nonsaturable reflectivity R_{ns} and the roll-over parameter F_2.

The saturation fluence F_{sat} is the fluence at which the reflectivity reduces to $1/e$ of its maximum. It also represents the point at which the population inversion inside the active region becomes saturated, therefore it is closely tied to the material properties of the active region.

The small signal reflectivity R_{ss} refers to the reflectivity at low probe fluence, where the gain is not significantly saturated. In this regime nonlinear effects are minimal and the reflectivity can be consider the be in the linear regime and the small signal approximation can be applied and the small signal gain can be calculated as $g_{ss} = R_{ss} - 100\%$.

The nonsaturable reflectivity R_{ns} arises from absorption and scattering at impurities and interfaces inside the VECSEL structure. This limits the maximum

performance of the VECSEL, thus reducing defect during the growing process is important. Since this effect is associated with imperfection and reflection inside the structure it remains relatively constant for different probe fluences.

The roll-over parameter F_2 describes further absorption from two photon absorption or higher order effects resulting in a strong decrease in the reflectivity at high fluences.

Figure 1.2 shows the key parameters and the fitted model with and without accounting for the roll-over for a measurement of a VECSEL with an integrated pump DBR.

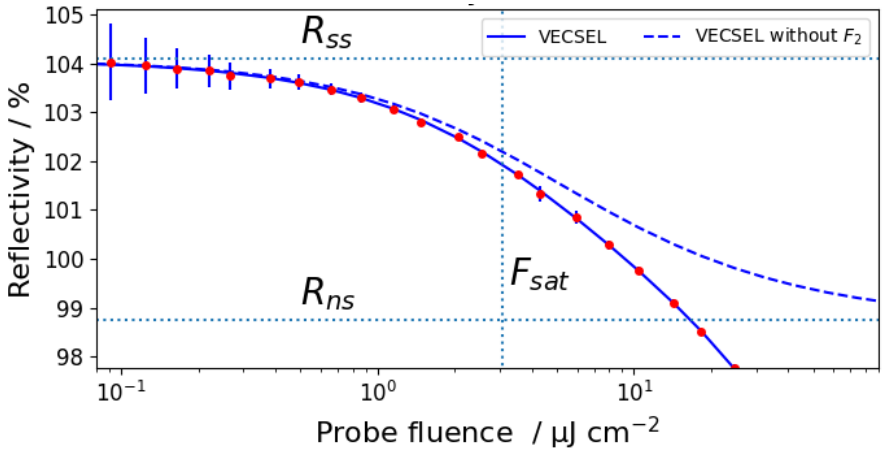

Figure 1.2: Nonlinear reflectivity measurement for a diamond backed VECSEL with integrated pump DBR versus probe fluence. The data is shown with the fitted model utilizing Eq. (1.1) and the same model without the roll over parameter F_2. Additionally the different parameters R_{ss}, R_{ns} and F_{sat} are visualized.

Chapter 2

Methods

In order to accurately determine the characteristic parameters of a VECSEL chip, it is necessary to have an experimental setup that can measure a small change, in the order of 0.1 % in the reflectivity over a dynamic range of about 4 order of magnitude in pulse fluence. A dedicated setup fulfilling these criteria has been constructed and utilized by (INSERT HERE REFERENCES).

For the measurements, a total of 4 different VECSEL chip were used, with three of them having a different structure (further discussed in Section 2.1). We were interested on the impact of different pump powers and the temperatures on the characteristic parameters of the VECSEL across the three different structures. For this we measured the nonlinear reflectivity for each chip for 9 different pump powers in the range from 0 W to 32 W and for three temperatures −10 °C, 0 °C and 10 °C.

The subsequent section provide an overview of the different VECSEL structures, the measurement setup and the data processing method.

2.1 VECSEL Chips

TODO: redo design images maybe with legend? different colors?

The basic structure of a VECSEL gain chip is shown in Fig. 2.1. The main feature of the structure are as follows:

- Heat spreader: The heat spreader role is in dissipating the heat generated during the operation of the VECSEL chip to a Peltier-controlled copper heat-sink.
- Pump & laser DBR: The purpose of the two bottom mirrors is to reflect the laser light and the pump light. There are two main advantages to this

approach: firstly, because of higher absorption, there is a higher optical-to-optical efficiency due to the two passes through the active region, and secondly, there is less absorption in the mirror and in the heat sink, which results also in a higher efficiency and a higher maximum output power. The high reflectivity for two wavelengths is realized by using a distributed Bragg reflector (DBR)

- Active region: The purpose of the active region is the conversion of the pump light into the laser light. The gain medium in the active region is often composed of quantum wells or quantum dots.
- Anti-reflection coating: The anti-reflection section is optimized to reduce the otherwise large reflection from the air/GaAs interface

Below the three different structure of the VECSEL chips used in this work.

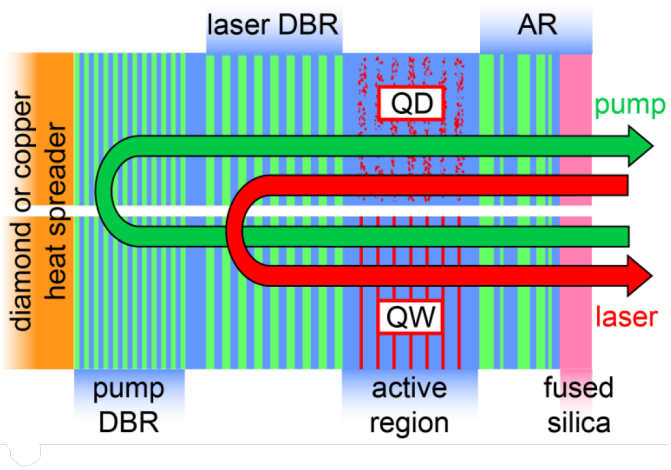

Figure 2.1: TODO: caption

No pump DBR chip, SV166

This structure has an antiresonant design and cooled from the backside by a copper heat spreader. The DBR consists of 19-pairs of $GaSb/AlAs_{0.08}Sb_{0.92}$ layers design around a wavelength of 2080 nm. The active region has 5×3 $In_{0.27}Ga_{0.73}Sb$ quantum wells (QW) placed at the maximum of the standing-wave cavity. Additional barriers layer made of $AlAs_{0.08}Sb_{0.92}$ are placed around the gain QW to increase the photoluminesence. The last layer is a PECVD coating made of Si_3N_4, which serves an an anti-reflection coating.

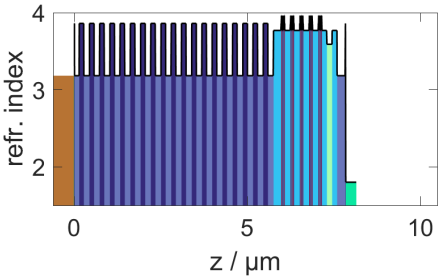

Figure 2.2: TODO: caption

Pump DBR chip, SV167

This is a similar structure as above but this time including an extra DBR for the pump wavelength of 1470 nm. The pump DBR is made of 10 layers of $Al_{0.2}As_{0.8}Sb/Al_{0.15}Ga_{0.85}AsSb$. For the thickness of the layers the 45° incident of the pump beam had to be accounted for. This structure was measured twice but for different heat spreaders, one made of copper and the other of diamond, to observe and compare the influence of better thermal conductivity of the heat spreader.

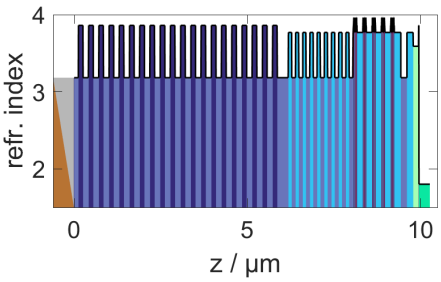

Figure 2.3: TODO: caption

Hybrid chip, SV165

This structure incorporated a hybrid metal-semiconductor Bragg reflector. It consisted of a 100 nm copper layer with 10.5 $AlAs_{0.08}Sb_{0.92}/GaSb$ layers. This allows for a thinner gain chip design of just under 5 µm compared to the other structures 7.5 µm resp. 10 µm for the pump DBR design. This lowered the thermal resistance of the device by 24 %. This structure also has a different active region made of 5×3 $In_{0.27}Ga_{0.73}Sb/GaSb$ QW.

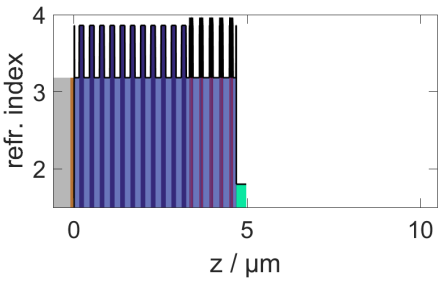

Figure 2.4: TODO: caption

2.2 Experimental setup

The experimental setup is depicted in Fig. 2.5. The setup is driven by a modelocked Ti:sapphire laser. The laser emits femtosecond pulses at a wavelength of 810 nm, with a repletion rate of 80 MHz and an average output power of 4 W. The laser beam then passes through an optical parametric oscillator (OPO), where the beam undergoes nonlinear frequency conversion resulting in two waves: an idler wave and a signal wave. The OPO idler wave can be tuned from 1.7 µm to 4 µm and has a maximum output power of 650 mW. The idler has been tuned to a specific wavelength of 2071.7 nm and was stabilized using an integrated automated feedback loop.

To further achieve a wide range of pulse fluences, the laser beam is directed through two wire-grid polarizers. One of the polarizers is placed on a controllable rotation stage to adjust the beam attenuation. The wire-grid polarizers have a broad range of attenuation across different wavelengths and do not alter the beam

path during rotation. After the attenuation stage, the beam passes through a beamsplitter, which separates it into two arms: the reference arm and the sample arm.

The reference arm contains a high-reflection mirror of known reflectivity from which the leaking signal is collect in a photo diode to monitor the fluence during a measurement. The VECSEl chip is placed at the end of the sampel arm. Before the beam is incident on the VECSEL, a focusing lens is used to achieve higher fluences on the VECSEL. The VECSEL is probed under a direct incidence angle, and its reflection is collected using the same lens. Both beams are recombined at the beamsplitter and direct to an integrating sphere photodiode to measure the total reflected power. The pump beam enters from the side at a 30° angle and is shown in green.

To measure the different signals from the two different arms and also measure the photoluminescence (PL) signal of the pumped VECSEL chips, two choppers are used. The two choppers separte the signals in time allowing to measure the signals with the same detector. The choppers are phase locked and chopper 2 is run at half of the frequency of chopper 1, specifically at 55 Hz. Chopper 2 is placed in the beam path before the attenuator to block the beam during every second cycle of chopper 1. This allows to isolate the PL signal. Chopper 1 is placed such that both arms can be intercepted by the blades, enabling the passage of light from both or either of the arms. During one cycle of chopper 2, five distincte state can occur, each allowing for a different measurement configuration:

1. Only the sample signal, composed of the photoluminescence and the sample signal (S+PL)
2. Both arms are open, allowing the compined singal from the sample and reference arm (S+PL+M)
3. Only the reference signal (M)
4. Both arms are blocked and only the background signal from the detector is measured (Z)
5. The probe beam gets blocked and only the (PL) signal is measured

To obtain the reflectivity from the VECSEL, the (PL) and the background signal (Z) are substracted from the sample signal (S+PL). The resulting value is then compared the reference measurement (M). This yields a scaling factor R, which then can be used to calculate the reflectivity based on the known reflectivity of the reference mirror. To obtain accurate measurement point, 200 such signal iteration are averaged together for the final measurement point.

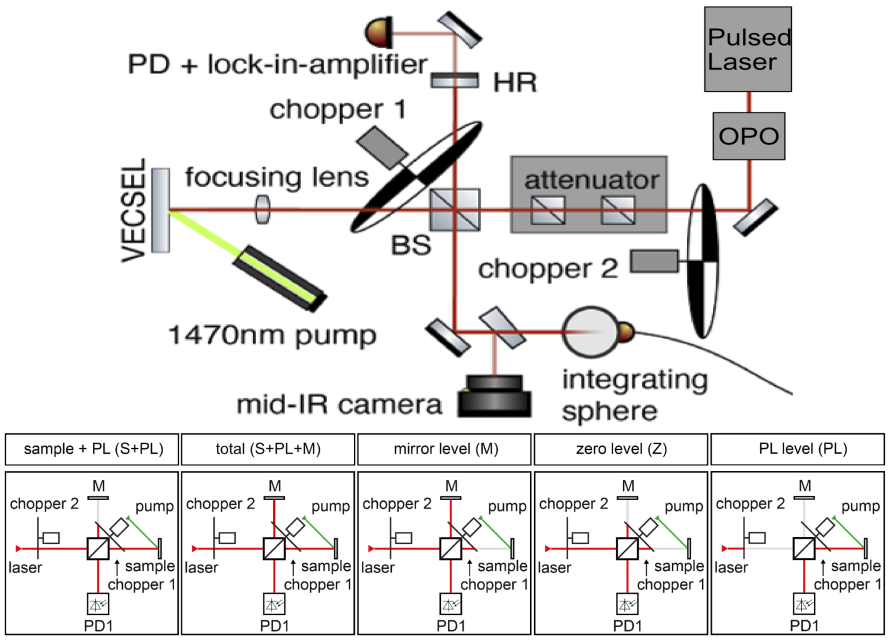

Figure 2.5: On top: Experimental Setup for gain characterization of VECSEL chips. The laser source is a tunable optical parametric oscillator pumped by a modelocked Ti:sapphire laser. An attenuation stage controls the incidient probe fluence on the VECSEL. The pump beam enters the setup at a 30° angle. Two choppers, phase-locked and operating at different frequencies, are positioned to differentiate signals and measure photoluminescence (PL) emitted by the pumped VECSEL chip. The figure showcases the key components and their relative positions within the experimental setup. On bottom: Visualization of the five different configuration of the two choppers and the measured signal, adjusted from REFERENCE.

2.2.1 Automation of the pump power

To improve the time efficiency and increase the unattented measuring time of the experimental setup, the control of the pump power has been automated. In the original setup, the pump power of the laser diode was controlled over a Delta Elektronika SM 18-50 DC power supply, which can deliver up to 50 A at up to 18 V. The power supply was connected over a serial interface controller to a computer and be integrated into the already existing user interface of the measurement setup. To implement the control of the pump, a new text field has been added to the user interafce where a list of current values for the power supply can be added. Instead of specifiying power values directly, the decisionaws made to enter current values instead due to the ptoential for exchaning the pump laser diode in the future, which would necessitate to adjust the controller in the software. The software then iterates over this lists and makes a complete measurement for each current value in the list. However, the full automation also required to adjust the signal processing algorithm of the software, which will be discussed in the next section.

a) b)

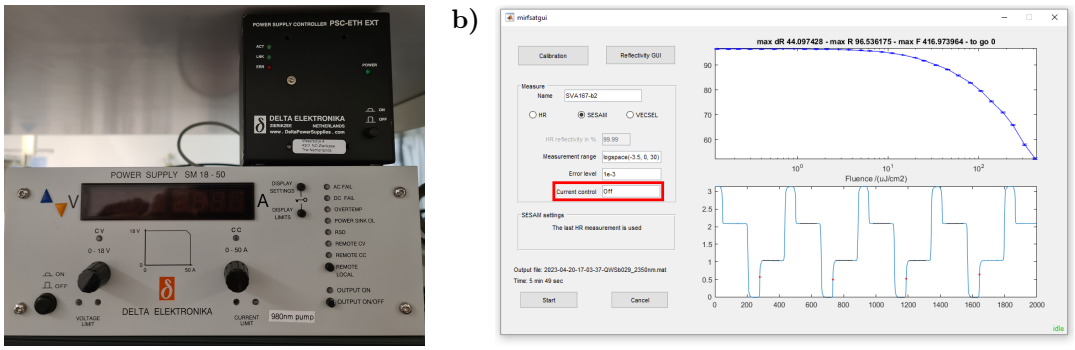

Figure 2.6: TODO: ADJUST SOFTWARE PICTURE AND WRITE CAPTION

2.3 Signal processing algorithm

In Fig. 2.7 the signal of the photodiode is shown for one cycle of chopper 2, as described in Section 2.2. The five signal levels resulting from the different chopper configuration are clearly distinguishable. To process the signal, the following algorithm had been used. Initially, , for example at 97 %, the software identifies trigger points when the signal falls below this level. Ideally, the triggering occurs at the falling edge of the total signal peak. The software utilizes these trigger points to determine the locations of the other signal levels and calculates the mean values of the flat levels. From these the software computes the sample reflectivity using the method outlined at the end of Section 2.2.

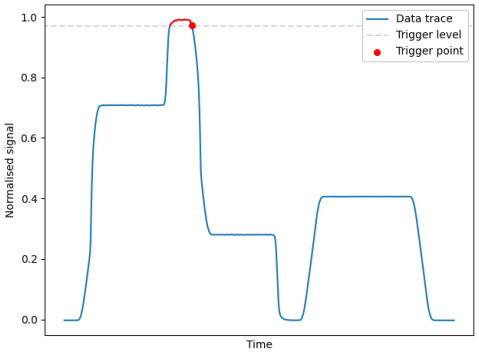

Figure 2.7: Illustration of original algorithm

However, this method exhibits some limitations when used for the automation for the setup. These limitations arise from the possibility to have multiple triggers in a single cycle, resulting in unusable measurement data and necessitating to manually adjusting the trigger and redoing the measurement. Such a manual process is counter productive to the aim of automation. To address this issue, it is essential to investigate the underlying caus

For one, there is the nature of the measured signal. Since all levels are measured simultaneously and with the same detector, their signal strength are in relation to each other. As a result, high variations in signal levels occur during a measurement, as illustrated in Fig. 2.8. Since measurements are conducted for different pump powers, the influence of the PL has to be taken into ac-

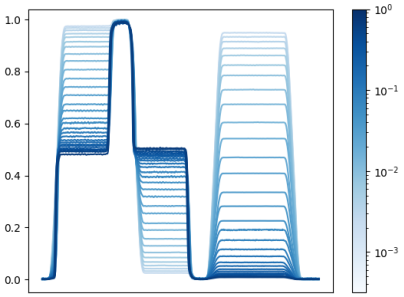

Figure 2.8: Signal for a fixed pump power and increasing amount of fluence. (NEED TO ADD AXIS LABEL TO IMAGE)

count. Initially, at low probe fluences, the PL signal dominates, requiring to set a trigger level to ensure triggering on the total level rather than the PL level.

To address these mistriggering cases, the following method has been implement which has also been illustrated in Fig. 2.9. By utilizing the approach described above but with a lower triggering value of 80 %, avoids triggering on a noisy total level but allows for triggering on both the total peak and the PL peak. Additionally, this introduces the risk of triggering on a noisy signal level that may lay close to the trigger level during a measurement. To address this, neighbouring points (small red dots in Fig. 2.9) of the triggers are examined and ensuring that the signal level is descending. Finally, we verify that we are on the total peak by requiring that a maximum value of the signal is in close proximity (orange shaded area in Fig. 2.9) to the trigger point.

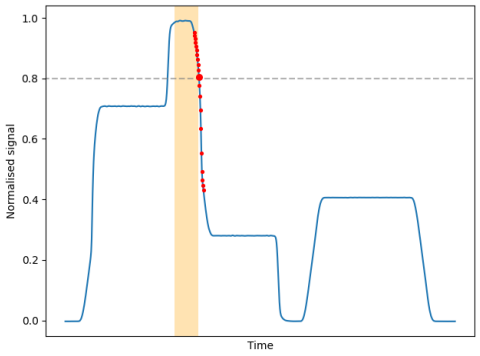

Figure 2.9: Illustration of improved algorithm

Using this method allowed for the automated measurement process to successfully be finished. Resulting in a decease of 5% in measurement time and the fully autonomous measuring of data.

Chapter 3

Results and Discussion

3.1 Measurement results

3.1.1 Saturation fluence F_{sat}

3.1.2 Small signal Reflectivity R_{ss}

3.1.3 Roll over parameter F_2

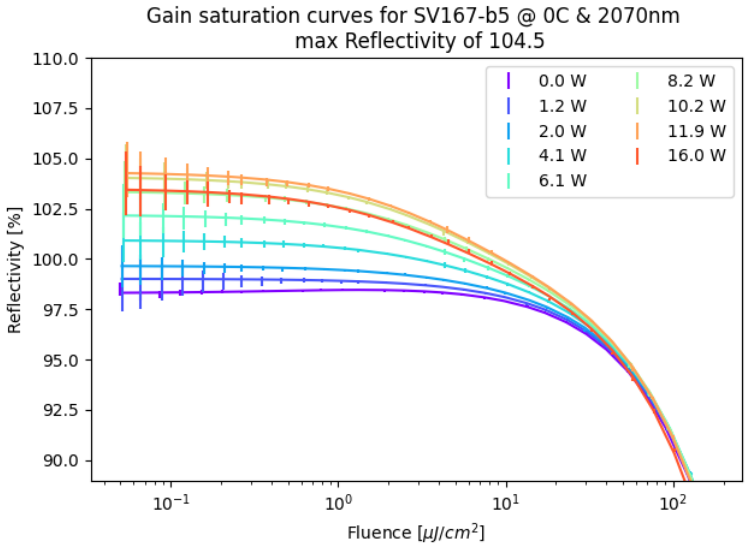

Figure 3.1

3.1.4 Overview

In Fig. 3.1 the result of the 0 °C measurement can be seen.

Chapter 4

Conclusion and Outlook